GEOPHYSICS, VOL. 84, NO. 6 (NOVEMBER-DECEMBER 2019); P. 1–7, 10 FIGS., 1 TABLE.
10.1190/GEO2018-0818.1

# Microseismicity caused by injection of water in a gas-saturated reservoir

Lucas A. Macias[1], Juan E. Santos[2], Gabriela B. Savioli[1], and José M. Carcione[3]

## ABSTRACT

Microseismic events along preexisting zones of weakness occur in a reservoir due to pore pressure buildup and fracturing during fluid injection. We have used a multiphase fluid-flow numerical simulator to model water injection in a gas reservoir. Previous studies generally consider a single fluid, in which the relative permeabilities and capillary pressure play no role. We analyze the effects of partial saturation on the injection process. On the basis of a spatial distribution of weak stress zones and a threshold pore pressure, the simulator models fluid transport in the formation and allows us to obtain the spatiotemporal distribution of the microseismic events. We consider uniform and fractal distributions of the pore pressure at which microearthquakes are triggered. We analyze the influence of the initial water saturation and the presence of preexisting natural fractures, as well as the effect of updating the rock properties after the microseismic events occur. Moreover, we perform simulations in a low-permeability reservoir in which the borehole pressure increment generates a system of fractures that propagate into the reservoir. The importance of considering two-phase fluid flow resides in the fact that partial saturation greatly affects the trigger time evolution. This is mainly due to the difference in compressibility of the two phases.

## INTRODUCTION

Fluid injection has been widely used in the petroleum industry for secondary or enhanced oil recovery as well as for hydraulic fracturing treatments. The process of hydraulic fracturing allows us to generate fractures or to connect already existing natural fractures thus creating a pathway by which the hydrocarbons can flow to the wellbore (Riahi and Damjanac, 2013). When it comes to unconventional reservoirs (tight or shale), this technique is necessary for the well to become productive (Nagel et al., 2013).

As a result of the injection process, the pore pressure buildup within the formation leads to a decrease of the effective stress, causing the zones of weakness to break down; consequently, P- and S-waves are emitted (Rutqvist et al., 2015). This passive seismic emission can be used to monitor the overall process. Longer term microseismic monitoring has been used to estimate fracture geometry and reservoir properties as permeability (Shapiro et al., 1997, 2005; Carcione et al., 2015). This analysis is usually performed by adjusting the trigger envelope curve and obtaining the associated hydraulic diffusivity parameter (Rothert and Shapiro, 2003). Other authors have presented rigorous models of hydraulic fracturing (Wangen, 2011) based on Biot's equation and a finite-element representation of the fracture pressure.

The purpose of our work is to apply a two-phase fluid flow simulator to describe water injection in a gas reservoir. We consider a reservoir with low permeability but high enough so that the injected fluid can leak into the formation. As the fluid is being injected, the pressure builds up and breaks down the weaker zones becoming microearthquakes sources. For the breakdown criteria, we use a simplified single threshold criterion considering only tensile failure as a consequence of the injection.

Using this approach, we evaluate the influence of different variables, such as the breakdown pressure and initial water saturation, the existence of natural high-permeability paths, and the effect of porosity and permeability variation in the fractured zones.

## TWO-PHASE SIMULATOR

This section describes the two-phase fluid-flow model used to simulate water injection into a gas reservoir, and the trigger criterion

Manuscript received by the Editor 12 December 2018; revised manuscript received 11 May 2019; published ahead of production 22 July 2019.
[1]Universidad de Buenos Aires, Facultad de Ingeniería, Instituto del Gas y del Petróleo, Laboratorio de Ingenier a de Reservorios, Av. Las Heras 2214 Piso 3, C1127AAR, Buenos Aires, Argentina. E-mail: lmacias@fi.uba.ar; gsavioli@fi.uba.ar.
[2]Universidad de Buenos Aires, Facultad de Ingeniería, Instituto del Gas y del Petróleo, Laboratorio de Geofísica Numérica, Av. Las Heras 2214 Piso 3, C1127AAR, Buenos Aires, Argentina and Purdue University, Department of Mathematics, West Lafayette, Indiana, USA. E-mail: santos@math.purdue.edu.
[3]Istituto Nazionale di Oceanografia e di Geofisica Sperimentale (OGS), Borgo Grotta Gigante 42c, 34010 Sgonico, Trieste, Italy. E-mail: jose.carcione@gmail.com.

to obtain the distribution of the microearthquake sources. A list of symbols is listed in Appendix A.

## Water injection model

Our first aim is to model the simultaneous flow of gas and water in a reservoir. This is achieved by solving the differential equations that describe the two-phase fluid flow in porous media (Aziz and Settari, 1985). These equations, obtained by combining the mass conservation equations with Darcy's empirical law, are

$$\nabla \cdot \left( \underline{\kappa} \frac{k_{rg}(S_w)}{B_g \eta_g} \nabla p_g \right) + \tilde{q}_g = \frac{\partial \left[ \phi \left( \frac{S_g}{B_g} \right) \right]}{\partial t}, \tag{1}$$

$$\nabla \cdot \left( \underline{\kappa} \frac{k_{rw}(S_w)}{B_w \eta_w} \nabla p_w \right) + \tilde{q}_w = \frac{\partial \left[ \phi \left( \frac{S_w}{B_w} \right) \right]}{\partial t}, \tag{2}$$

where $g$ and $w$ denote the gas and water phases, respectively, and the unknowns are the fluid pressures $p_\beta$ and saturations $S_\beta$ ($\beta = w, g$). Moreover, $\tilde{q}_\beta$ is the injection flow rate per unit volume, $\eta_\beta$ is the viscosity, $\phi$ is the porosity, $\underline{\kappa}$ is the absolute permeability tensor, and $k_{r\beta}(S_w)$ is the relative permeability, which is a function of saturation. Finally, $B_g$ and $B_w$ are the PVT parameters, which are the gas formation volume factor and water formation volume factor, respectively. These equations are obtained by assuming that there is no mass transfer between gas and water phases. Two algebraic equations relating the saturations and pressures complete the system:

$$S_w + S_g = 1, \qquad p_g - p_w = P_C(S_w), \tag{3}$$

where $P_C(S_w)$ is the capillary pressure function.

This is a nonlinear system due to the dependence of the relative permeabilities and the capillary pressure on the saturation. This approach differs from previous studies (Shapiro, 2015; Carcione et al., 2017), in which the nonlinearity of the flow equation is related to the dependency of the permeability on the pressure. One of our numerical examples considers a change in permeability when a pressure threshold is reached. However, this change in permeability is not represented in the model equations, but it is imposed externally.

Appendix B describes how the nonlinear differential equations 1 and 2 are obtained and solved.

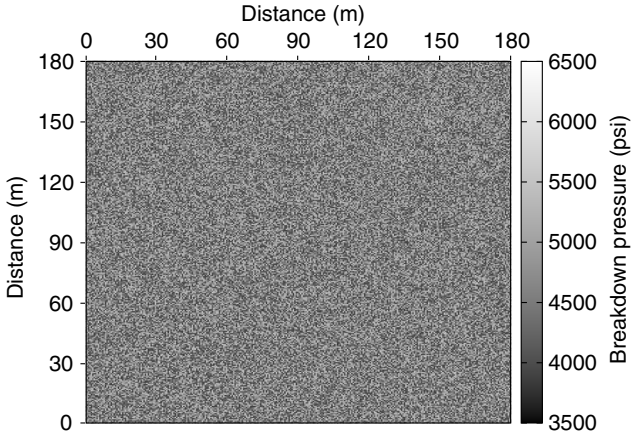


Figure 1. Fractal breakdown pressure distribution.

## Triggering criterion

To determine the microseismic emission zones, we apply a criterion based on a "breakdown pressure" ($P_{bd}$) defined as follows: When the pore pressure $p$ is greater than the breakdown pressure on a certain cell, it becomes a "microseismic source."

The term $P_{bd}$ can be computed from the in situ stress field, and a good estimation of the stress field is important. It requires surface seismic, sonic log, and VSP data. Many authors have developed different tools and techniques, combining well-log data and seismic information, to estimate the reservoir properties. Bosch et al. (2010, 2014) present a methodology in which the elastic properties are obtained by inverting seismic data. In addition, Curcio et al. (2016) develop a procedure using VSP data.

This single threshold criterion approach is similar to that described by Rothert and Shapiro (2003). In this case, we only consider tensile events, and the $P_{bd}$ is obtained from the horizontal stress $\sigma_H$ and the tensile stress of the rock $T_0$ (Economides and Hill, 1994) as

$$P_{bd} = 3\sigma_{H\,\min} - \sigma_{H\,\max} + T_0 - p_H, \tag{4}$$

where

$$\sigma_{H\,\max} = \sigma_{H\,\min} + \sigma_{\mathrm{Tect}}, \tag{5}$$

where $\sigma_{\mathrm{Tect}}$ being the tectonic stress contribution and $\sigma_{H\,\max}$ and $\sigma_{H\,\min}$ being the maximum and minimum horizontal stresses, respectively, obtained from the vertical stress $\sigma_V$ as

$$\sigma_{H\,\min} = \frac{\nu}{1-\nu}\sigma_V, \tag{6}$$

where $\nu$ is Poisson's ratio and $\sigma_V$ is calculated from the formation density $\rho_f$ as

$$\sigma_V = g \int_0^H \rho_f dH, \tag{7}$$

with $H$ indicating the formation depth and $g$ is the gravity constant.

## NUMERICAL EXAMPLES

We consider a 2D horizontal section of a gas reservoir with an extent of 180 m in the $x$-direction and 180 m in the $y$-direction. The reservoir is located at a depth of 3 km b.s.l. The simulation is performed by using a mesh with equally spaced blocks in each direction, distributed in 300 cells in the $x$-direction and 300 cells in the $y$-direction. We designed a reservoir with a permeability of 0.1 mD and 8% of porosity. In our first analysis, we maintain these reservoir properties as constants; i.e., we assume that when the breakdown pressure is reached, the properties are not modified. We also assume a fractal distribution for $P_{bd}$ based on the von Kármán correlation function (Carcione and Gei, 2009) as shown in Figure 1. The fractal breakdown pressure is obtained with the following relation:

$$P_{bd}(x,z) = \langle P_{bd} \rangle + f(x,z), \tag{8}$$

where $\langle P_{bd} \rangle$ denotes the spatial average of $P_{bd}(x, z)$ and $f(x, z)$ is a fractal field representing the spatial fluctuation of $P_{bd}(x, z)$, for which the spectral density $S_d(r_x, r_z)$ is given by (Frankel and Clayton, 1986)

$$S_d(r_x, r_z) = N_0(1 + R^2\alpha^2)^{-(H+E/2)}, \quad (9)$$

where $R = \sqrt{r_x^2 + r_z^2}$ is the radial wavenumber, $\alpha$ is the correlation length, $H$ is a self-similar coefficient ($0 < H < 1$), $N_0$ is a normalization constant, and $E$ is the Euclidean dimension. The von Kármán correlation describes a self-affine, fractal process of fractal dimension $D = E + 1 - H$ at a scale smaller than $\alpha$. For this first application, we take $E = 2$ and $D = 5$ and $\langle P_{bd} \rangle = 5000$ psi (34.5 MPa). The correlation length value was taken to be 1% of the domain size. We generated a breakdown pressure field by choosing the variance parameter in the fractal generator (200,000 psi$^2$).

Water injection simulation is performed at a constant flow rate of 0.15m$^3$/s at the injection point located in the center of reservoir with the BOAST simulator (Table 1). Figure 2 shows the spatial distribution of triggers after 10 h of the fracking process. A flow rate of 0.15 m$^3$/s on a 10 h interval is considered for all experiments. This is consistent with values for water injection into low-permeability reservoirs during fracking processes.

We can see that the pore pressure increase due to water injection generates fractures in the reservoir in weak zones around the well. The spatial distribution of fractured cells observed in Figure 2 corresponds to the end of the fracking process, in which each particular trigger occurred at a different time. This trigger time evolution can be observed in Figure 3 as a cloud of crosses (fractal $P_{bd}$), where the maximum distance to the well reached after 10 h of injection is 12.76 m.

If instead of assuming a fractal distribution for the breakdown pressure, we use a homogeneous distribution taking the minimum value of the fractal case (4000 psi/27.6 MPa), we obtain the trigger time evolution result depicted in Figure 3 as a dotted curve of points (homogeneous $P_{bd}$). This curve is the envelope of all trigger events generated in the previous case.

Then, we study the effect of modifying the local properties after the pressure reaches the $P_{bd}$ value on a certain cell. When this happens, the cell porosity and permeability values are increased. The new porosity and permeability values are assigned by assuming an average between the existing properties of the formation and those of the fracture. The fluid-flow model does not compute these new values, but they are instead assigned as a parameter for each time step when the cell is considered fractured. Because the focus of this study is to demonstrate that any change in the local properties might alter the shape or size of the microearthquakes' source distribution, we do not put the emphasis in determining the exact values of the new porosity or permeability of the cell. The presence of proppant is accounted for by assigning new values of porosity and permeability of the fracture. The values used to update the cell properties after fracturing were 50 mD for permeability and 50% for porosity.

In this case, the behavior is slightly different, and it can be seen in Figure 4, which shows the trigger time evolution for the constant and variable properties assuming a uniform distribution of $P_{bd} = 4000$ psi (27.6 MPa). This difference can be explained by the fact that an increment in porosity and permeability produces a pressure drop. This decrease slows down the pressure front, which, in turn, delays the triggers.

**Table 1. Model parameter case 1.**

| | | | |
|---|---|---|---|
| $\phi$ | 8% | $\tilde{q}_w$ | 0.15m$^3$/s |
| $\kappa$ | 0.1 mD | Inj. time | 10 h |
| $\langle P_{bd} \rangle$ | 34.5 MPa | — | — |

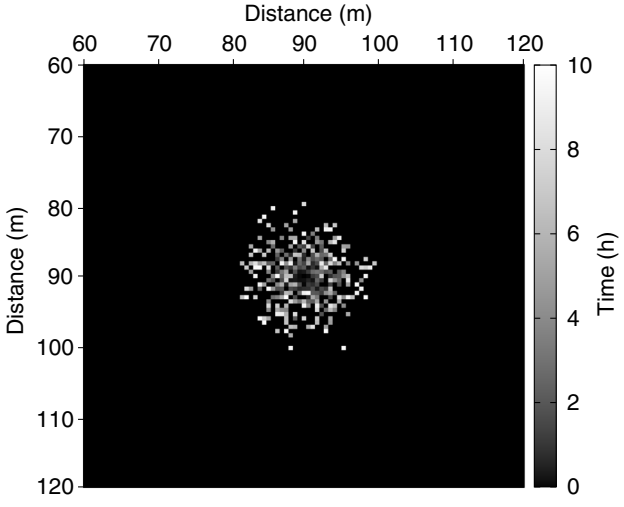


Figure 2. Location of the microseismic sources obtained after 10 h of water injection.

## BREAKDOWN PRESSURE AND INITIAL WATER SATURATION EFFECT

The value used as the breakdown pressure depends on several factors as mentioned above, such as formation density, tensile stress of the rock, and tectonic stress among others. It is our objective to determine whether an accurate value of $P_{bd}$ is needed when simulating the fracture front, or an approximation is sufficient. Hence, it is important to consider the effect that this parameter has on the

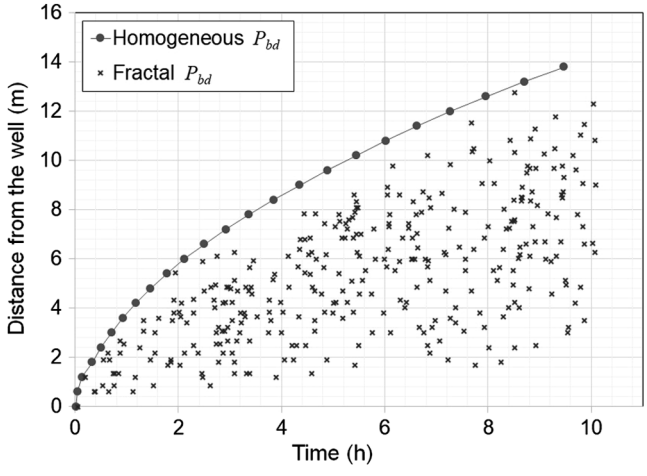


Figure 3. Comparison between the homogeneous and fractal breakdown pressure $P_{bd}$ distribution.

fracture evolution and to understand the sensitive of the front to changes in the breakdown pressure. To evaluate this effect, we run four simulations for different values $P_{bd}$ of 4000 psi (27.6 MPa), 4500 psi (31.0 MPa), 5000 psi (34.5 MPa), and 5500 psi (37.9 MPa). These simulations are performed by assuming a uniform distribution of $P_{bd}$. The corresponding envelopes are shown in Figure 5.

It can be clearly observed that an increment of $P_{bd}$ not only slows down the triggering but also reduces the size of the fractured zone. In this case, the effect can be easily explained if we assume that within a certain region of the reservoir it is necessary to reach a higher pore pressure to fracture for higher $P_{bd}$ values. An increase of approximately 12% of $P_{bd}$ produces a 50% decrease in the distance to the well of the fracture front. On the other hand, a 37% increment of $P_{bd}$ leads to an 84% decrease in the region covered by the fractured zone.

Variable water saturation is another significant property. Five different initial water saturations are considered (0.1, 0.3, 0.5, 0.8, and 1.0), while maintaining a constant $P_{bd}$ of 4000 psi (27.6 MPa) for all five cases. Figure 6 shows the envelope behavior for the different saturations.

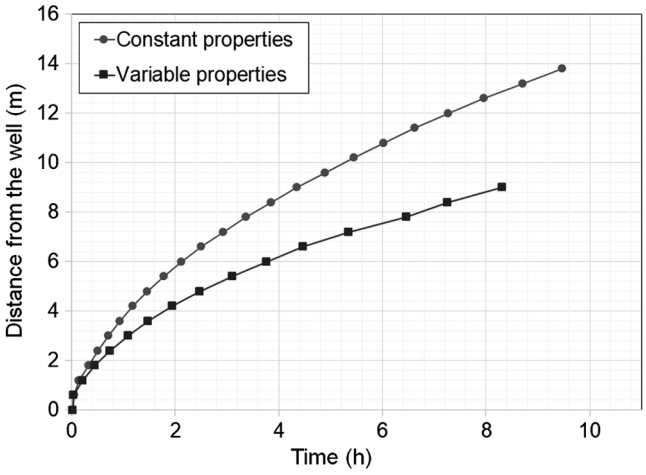


Figure 4. Location of the events as a function of the emission time, corresponding to a homogeneous distribution of the breakdown pressure, with constant and variable properties.

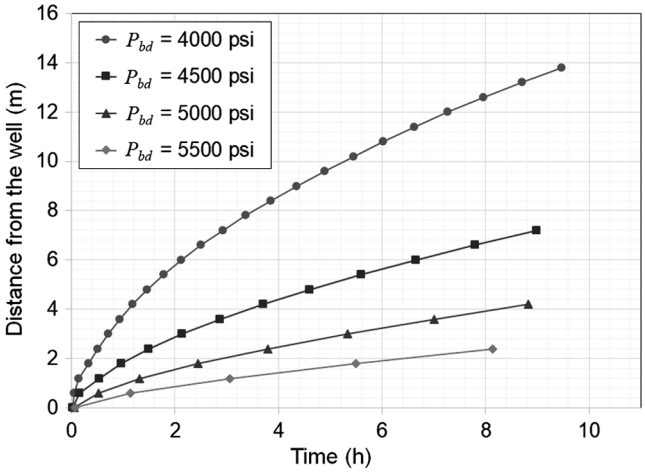


Figure 5. Breakdown pressure $P_{bd}$ effect on the trigger distribution.

An increment of initial water saturation generates the opposite effect; that is, the fracture front evolution is accelerated and the fractured zone increases. This can be explained if we take into account that the pore pressure increases with the increasing water saturation. Figure 6 shows the importance of considering two-phase fluid flow because water injection into a gas reservoir greatly affects the trigger time evolution. This is mainly due to the difference in compressibility of the two phases.

Any values of $P_{bd}$ and $S_{wi}$ can be used in the model, but higher values of $P_{bd}$ will not trigger microseismic events, and lower values will trigger many events. Then, it is important to define the appropriate working range considering the properties of the reservoir under study.

## EFFECT OF PREEXISTING NATURAL FRACTURES

In this section, we analyze the case in which the reservoir has natural fractures before starting the fracking process and the influence of such natural fractures on the evolution of the induced fractures. For this purpose, we incorporate zones of high permeability, as shown in Figure 7. These zones model the natural fractures. Because the mesh is fixed and the size of the cells is much larger than that of a natural fracture, we randomly choose a series of cells placed along parallel lines close to the injection point, and we assign them a value of permeability greater than that of the formation, weighted together with the high permeability that a natural fracture would have.

In our simulation, we model closed boundaries on the simulation zone, whereas the fracture boundaries are open, except those coinciding with the zone boundaries. We avoid the border effect by ensuring that the pressure and saturation changes do not reach the boundaries. In our model, the fractures are part of the simulation grid, allowing fluid to flow from adjacent cells. If we consider closed fracture boundaries, we do not expect very dissimilar results because the reservoir permeability is low, with a fluid flow dominant in the fracture and a low flow into the matrix.

Figures 8 and 9 show the maps of the fractured zone after 10 h of injection without and with natural fractures. There is a decrease in the size of the fractured zone due to the presence of natural

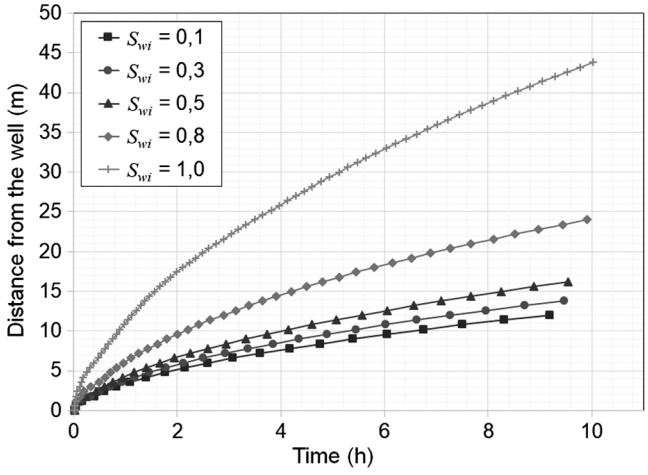


Figure 6. Initial water saturation $S_{wi}$ effect on the trigger distribution.

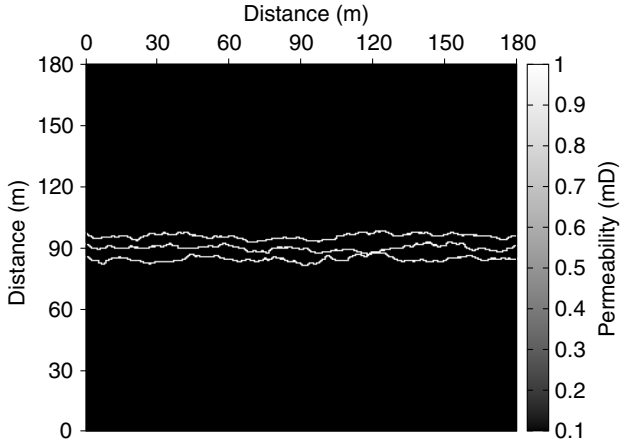


Figure 7. Permeability map with natural fractures.

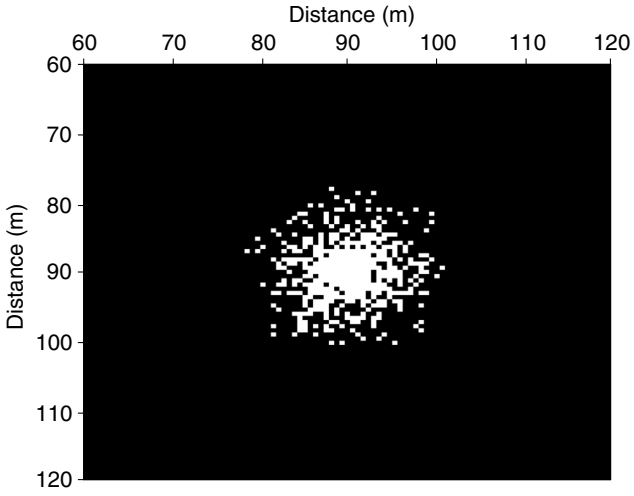


Figure 8. Fracture map without natural fractures.

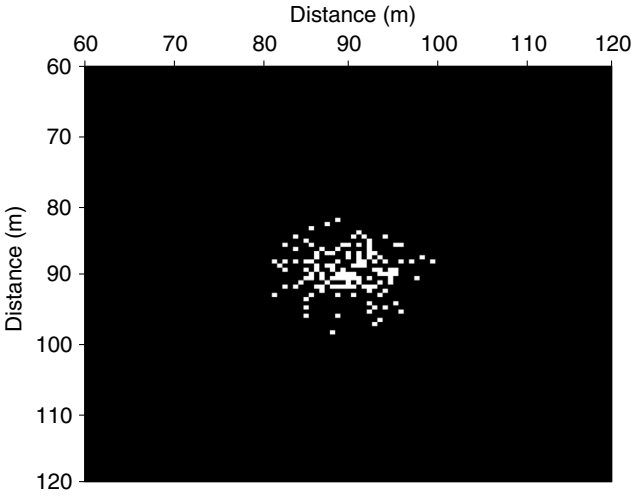


Figure 9. Fracture map with natural fractures.

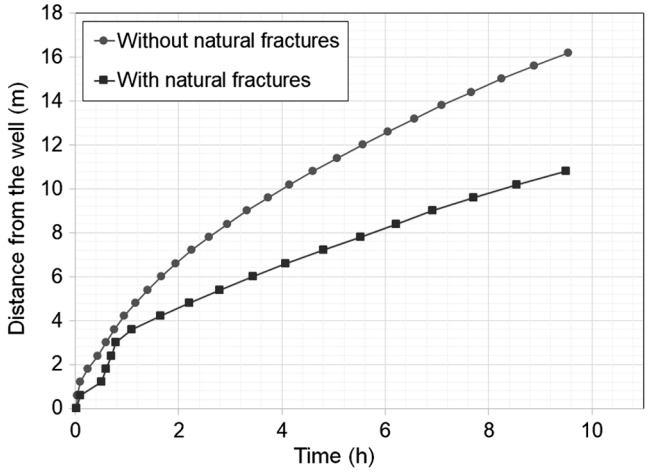


Figure 10. Effect of the natural fractures on the trigger distribution.

fractures. The natural fractures allow water to flow more easily; thus, pressure increases slowly, which in turn decreases the number of induced fractures. The effect of the reduction of the fractured zone, along with the decrease of the trigger events, can be seen in the trigger event time distribution (see Figure 10).

## CONCLUSION

The model presented here allows us to generate microearthquake sources maps in a reservoir saturated with two phases during the fracking process. We analyze the influence of the rock stresses, the initial water saturation, and the presence of natural fractures on the time-spatial distribution of the microseismic sources.

It can be observed that an increment of the breakdown pressure not only slows down the triggering but also reduces the size of the fractured zone. An increment of initial water saturation induces the opposite effect; i.e., the fracture front evolution is accelerated and the fractured zone increases. Moreover, there is a decrease in the size of the fractured zone due to the presence of preexisting natural fractures. These fractures allow water to flow more easily; thus, pressure increases slowly, which in turn decreases the number of induced fractures.

This model is also valid to analyze the effect of other fluids or reservoir properties such as permeability, porosity, rock formation compressibility, fluid compressibility, relative permeability curves, capillary pressure curves, and injection rates.

Although our work does not consider changes of the local tensions caused by the microseismic events, the model can incorporate this by modifying the $P_{bd}$ after each event on the fracture cell and those adjacent to it. Our study considers two cases: (1) We do not modify the porosity and permeability after each microseismic event and (2) we modify these properties. In case 1, we expect the slope of the envelope curve to increase with the number of events, but the pressure and saturation distributions are not affected. In case 2, we expect an effect similar to the generation of natural fractures, in which the simulation yields weaker zones.

This work is a starting point that will enable us to generate seismic images produced by the fracture events that are obtained as an output of the model. Furthermore, we can obtain the fracture map from a set of real seismic images by using inversion algorithms. We point out the importance of considering two-phase flow or,

in general, multiphase fluid flow when studying the behavior of induced fractures during the hydraulic fracture processes.

## ACKNOWLEDGMENTS

This work is partially funded by the Agencia Nacional de Promoción Científica, Argentina (grant no. PICT-2015-1909), Universidad de Buenos Aires, Secretaría de Ciencia y Técnica (grant no. UBACyT 20020160100088BA), and a Peruilh grant provided by the Facultad de Ingeniería — Universidad de Buenos Aires.

## DATA AND MATERIALS AVAILABILITY

Data associated with this research are confidential and cannot be released.

## APPENDIX A

## NOMENCLATURE

| | |
|---|---|
| $B_w$ | water formation volume factor |
| $B_g$ | gas formation volume factor |
| $c_w$ | water compressibility |
| $c_f$ | formation compressibility |
| $c_g$ | gas compressibility |
| $c_t$ | total compressibility |
| $g$ | gravity constant |
| $k_{r\beta}(S_w)$ | $\beta$ phase relative permeability function |
| $p_\beta$ | $\beta$ phase pressure |
| $p_H$ | hydrostatic pressure |
| $P_{bd}$ | breakdown pressure |
| $P_C(S_w)$ | capillary pressure function |
| $\tilde{q}_\beta$ | $\beta$ phase injection flow rate per unit volume |
| $S_\beta$ | $\beta$ phase saturation |
| $S_{wi}$ | initial water saturation |
| $T_0$ | tensile stress |
| $\underline{v}_\beta$ | Darcy phase velocity |
| $\eta_\beta$ | $\beta$ phase viscosity |
| $\underline{\kappa}$ | absolute permeability tensor |
| $\nu$ | Poisson's ratio |
| $\rho_f$ | formation density |
| $\sigma_H$ | horizontal stress |
| $\sigma_{H\,\max}$ | maximum horizontal stress |
| $\sigma_{H\,\min}$ | minimum horizontal stress |
| $\sigma_V$ | vertical stress |
| $\sigma_{\text{Tect}}$ | tectonic stress |
| $\phi$ | porosity |

## APPENDIX B

## BLACK-OIL FORMULATION OF TWO-PHASE FLOW IN POROUS MEDIA

The simultaneous flow of water and gas is described by the well-known black-oil formulation (Aziz and Settari, 1985). This formulation uses, as a simplified thermodynamic model, the PVT data defined as

- $B_g$: gas formation volume factor
- $B_w$: water formation volume factor.

The formation volume factors of gas and water are defined as the ratio of the volume of each phase at the reservoir temperature and pressure to the volumes at the standard surface temperature and pressure (15°C and 1 atm).

The conversion of compositional data from equations of state into the black-oil PVT data is based on an algorithm developed by Hassanzadeh et al. (2008). The mass conservation equation for each component (gas and water) can be expressed as

$$-\nabla\cdot\left(\frac{1}{B_g}\underline{v}_g\right)+\tilde{q}_g=\frac{\partial\left[\phi\left(\frac{S_g}{B_g}\right)\right]}{\partial t}, \tag{B-1}$$

$$-\nabla\cdot\left(\frac{1}{B_w}\underline{v}_w\right)+\tilde{q}_w=\frac{\partial\left[\phi\left(\frac{S_w}{B_w}\right)\right]}{\partial t}, \tag{B-2}$$

where $g$ and $w$ denote the gas and water phases, respectively, $\phi$ is the porosity, $\underline{v}_\beta$ is the Darcy phase velocity, $S_\beta$ is the saturation, and $\tilde{q}_\beta$ is the injection flow rate per unit volume, with $\beta = w, g$.

The Darcy phase velocities in an horizontal domain can be expressed by Darcy's empirical law as

$$\underline{v}_g=-\underline{\kappa}\frac{k_{rg}(S_w)}{\eta_g}\nabla p_g, \tag{B-3}$$

$$\underline{v}_w=-\underline{\kappa}\frac{k_{rw}(S_w)}{\eta_w}\nabla p_w, \tag{B-4}$$

where $p_\beta$ is the fluid pressures, $\eta_\beta$ is the viscosity, $\underline{\kappa}$ is the absolute permeability tensor, and $k_{r\beta}(S_w)$ is the relative permeability that is a function of saturation. Combining the mass conservation equations (equations B-1 and B-2) with Darcy's law (equations B-3 and B-4), we obtain equations B-5 and B-6 (equations 1 and 2 in the "Water injection model" subsection)

$$\nabla\cdot\left(\underline{\kappa}\frac{k_{rg}(S_w)}{B_g\eta_g}\nabla p_g\right)+\tilde{q}_g=\frac{\partial\left[\phi\left(\frac{S_g}{B_g}\right)\right]}{\partial t}, \tag{B-5}$$

$$\nabla\cdot\left(\underline{\kappa}\frac{k_{rw}(S_w)}{B_w\eta_w}\nabla p_w\right)+\tilde{q}_w=\frac{\partial\left[\phi\left(\frac{S_w}{B_w}\right)\right]}{\partial t}. \tag{B-6}$$

Two algebraic equations relating the saturations and pressures complete the system:

$$S_w+S_g=1,\qquad p_g-p_w=P_C(S_w), \tag{B-7}$$

where $P_C(S_w)$ is the capillary pressure function.

Two types of multiphase flow functions appear on the system of equations (equations B-5–B-7): relative permeability and capillary pressure, where each one is a function of saturation.

The numerical solution of the system is obtained with the algorithm BOAST (Fanchi, 1997), which solves the differential equations using implicit pressure explicit saturation (IMPES), a finite-difference technique (Aziz and Settari, 1985). The basic idea of IMPES is to obtain a single pressure equation by a combination of the flow equations. Once pressure is implicitly computed, saturation is updated explicitly. We briefly describe IMPES for these particular systems (equations B-5–B-7). The first step is to obtain the pressure equation, combining flow equations: Equation B-5 multiplied by $B_g$ and equation B-6 multiplied by $B_w$ are added. In this way, the right side of the resulting equation is

$$B_g \frac{\partial\left[\phi\left(\frac{S_g}{B_g}\right)\right]}{\partial t} + B_w \frac{\partial\left[\phi\left(\frac{S_w}{B_w}\right)\right]}{\partial t}. \tag{B-8}$$

5 Using the chain rule to expand the time derivatives and after some computations and rearrangements, we obtain

$$\phi\left[\frac{1}{\phi}\frac{d\phi}{dp_w} + S_g\left(-\frac{1}{B_g}\frac{dB_g}{dp_w}\right) + S_w\left(-\frac{1}{B_w}\frac{dB_w}{dp_w}\right)\right]\frac{\partial p_w}{\partial t}, \tag{B-9}$$

where all the time derivatives with respect to the saturation disappear.

Defining

- formation compressibility: $c_f = (1/\phi)(d\phi/dp_w)$
- gas compressibility: $c_g = -(1/B_g)(dB_g/dp_w)$
- water compressibility: $c_w = -(1/B_w)(dB_w/dp_w)$
- total compressibility: $c_t = c_f + S_g c_g + S_b c_w$.

The right side of the pressure equation is expressed as

$$\phi c_t \frac{\partial p_w}{\partial t}. \tag{B-10}$$

Finally, replacing $p_g$ by $p_w + P_C(S_w)$ in the left side of the combined equation, the following pressure equation in $p_w$ is obtained:

$$\begin{aligned} &B_g\left[\nabla\cdot\left(\underline{\kappa}\left(\frac{k_{rg}}{B_g\eta_g}\nabla p_w + \frac{k_{rg}}{B_g\eta_g}\nabla P_C\right)\right)\right] \\ &+ B_w\left[\nabla\cdot\left(\underline{\kappa}\frac{k_{rw}}{B_w\eta_w}\nabla p_w\right)\right] \\ &+ B_g\tilde{q}_g + B_w\tilde{q}_w = \phi c_t\frac{\partial p_w}{\partial t}. \end{aligned} \tag{B-11}$$

In the BOAST simulator, equations B-6 and B-11 are discretized using a block centered grid. The system is linearized by evaluating the pressure- and saturation-dependent functions (PVT parameters, viscosities, relative permeabilities, and capillary pressure) in the pressure and saturation values of the previous time step. The pressure equation is solved implicitly, applying a block successive over relaxation method to compute the linear system solution. The saturation equation is solved explicitly; therefore, stability restrictions are considered to select the time step (Savioli and Bidner, 2005).

## REFERENCES


Aziz, K., and A. Settari, 1985, Petroleum reservoir simulation: Elsevier Applied Science Publishers.

Bosch, M., D. Morales, Y. Gomez, T. Kazmierczak, T. Salinas, G. Alvarez, A. Moreno, Y. Pino, and E. Medina, 2014, Elastic seismic inversion and reservoir characterization in the Llanos Basin, Colombia: The Leading Edge, **33**, 734–744, doi: 10.1190/tle33070734.1.

Bosch, M., T. Mukerji, and E. Gonzalez, 2010, Seismic inversion for reservoir properties combining statistical rock physics and geostatistics: A review: Geophysics, **75**, no. 5, 75A165–75A176, doi: 10.1190/1.3478209.

Carcione, J. M., G. Currenti, L. Johann, and S. Shapiro, 2017, Modeling fluid injection induced microseismicity in shales: Journal of Geophysics and Engineering, **15**, 234–248, doi: 10.1088/1742-2140/aa8a27.

Carcione, J. M., F. Da Col, G. Currenti, and B. Cantucci, 2015, Modeling techniques to study $CO_2$-injection induced micro-seismicity: International Journal of Greenhouse Gas Control, **42**, 246–257, doi: 10.1016/j.ijggc.2015.08.006.

Carcione, J. M., and D. Gei, 2009, Theory and numerical simulation of fluid-pressure diffusion in anisotropic porous media: Geophysics, **74**, no. 5, N31–N39, doi: 10.1190/1.3192911.

Curcio, A., A. Grosso, R. Perez, and O. Barrios-Lopez, 2016, Anisotropy study of deep unconventional reservoir inverting walkaway VSP data, Argentina: 86th Annual International Meeting, SEG, Expanded Abstracts, 362–363, doi: 10.1190/segam2016-13577602.1.

Economides, M. J., and A. D. Hill, 1994, Petroleum production systems: Prentice Hall PTR.

Fanchi, J., 1997, Principles of applied reservoir simulation: Gulf Professional Publishing Company.

Frankel, A., and R. W. Clayton, 1986, Finite difference simulation of seismic wave scattering: Implications for the propagation of short period seismic waves in the crust and models of crustal heterogeneity: Journal of Geophysical Research, **91**, 6465–6489, doi: 10.1029/JB091iB06p06465.

Hassanzadeh, H., M. Pooladi-Darvish, A. Elsharkawy, D. Keith, and Y. Leonenko, 2008, Predicting PVT data for $CO_2$-brine mixtures for black-oil simulation of $CO_2$ geological storage: International Journal of Greenhouse Gas Control, **2**, 65–77, doi: 10.1016/S1750-5836(07)00010-2.

Nagel, N., F. Zhang, M. Sanchez-Nagel, and B. Lee, 2013, Numerical study of interaction between hydraulic fracture and discrete fracture network: Presented at the Quantitative Evaluation of Completion Techniques on Influencing Shale Fracture Complexity, INTECH.

Riahi, A., and B. Damjanac, 2013, Numerical study of interaction between hydraulic fracture and discrete fracture network: Presented at the Effective and Sustainable Hydraulic Fracturing, INTECH.

Rothert, E., and S. A. Shapiro, 2003, Microseismic monitoring of borehole fluid injections: Data modeling and inversion for hydraulic properties of rocks: Geophysics, **68**, 685–689, doi: 10.1190/1.1567239.

Rutqvist, J., A. P. Rinaldi, F. Cappa, and G. J. Moridis, 2015, Modeling of fault activation and seismicity by injection directly into a fault zone associated with hydraulic fracturing of shale-gas reservoirs: Journal of Petroleum Science and Engineering, **127**, 377–386, doi: 10.1016/j.petrol.2015.01.019.

Savioli, G., and M. S. Bidner, 2005, Simulation of the oil and gas flow toward a well — A stability analysis: Journal of Petroleum Science and Engineering, **48**, 53–69, doi: 10.1016/j.petrol.2005.04.007.

Shapiro, S., 2015, Fluid-induced seismicity: Cambridge University Press.

Shapiro, S. A., E. Huenges, and G. Borm, 1997, Estimating the crust permeability from fluid-injection-induced seismic emission at the KTB site: Geophysical Journal International, **131**, F15–F18.

Shapiro, S. A., S. Rentsch, and E. Rothert, 2005, Characterization of hydraulic properties of rocks using probability of fluid-induced microearthquakes: Geophysics, **70**, no. 2, F27–F33, doi: 10.1190/1.1897030.

Wangen, M., 2011, Finite element modeling of hydraulic fracturing on a reservoir scale in 2D: Journal of Petroleum Science and Engineering, **77**, 274–285, doi: 10.1016/j.petrol.2011.04.001.

# Queries

1. Please spell out PVT.
2. Please spell out VSP.
3. Please spell out BOAST.
4. Please check and confirm whether the "List of symbols" in Appendix A can be moved to a Nomenclature section.
5. Unnumbered equations are not allowed by SEG style, so we have renumbered the equation as well as the text citation. Please check the renumbering and the text mentions of the equations.

# Funding Information

The following agencies have been identified as providing funding for your article. Please review the information carefully. If any changes are required, please submit those along with your other corrections to this article.

- Agencia Nacional de Promoción Científica, Argentina (FundRef Registry ID: http://dx.doi.org/10.13039/501100007351)
- Universidad de Buenos Aires Secretaría de Ciencia y Técnica (FundRef Registry ID: http://dx.doi.org/10.13039/501100006668)